ELSEVIER

International Journal of Mass Spectrometry 197 (2000) 263–278

International Journal of Mass Spectrometry

Frequency perturbation in nonlinear Paul traps: a simulation study of the effect of geometric aberration, space charge, dipolar excitation, and damping on ion axial secular frequency

S. Sevugarajan, A.G. Menon*

Department of Instrumentation, Indian Institute of Science, Bangalore 560012, India

Received 13 September 1999; accepted 8 December 1999

Abstract

This article develops an expression that relates perturbation in ion axial secular frequency to geometric aberration, space charge, dipolar excitation, and collisional damping in nonlinear Paul trap mass spectrometers. A multipole superposition model incorporating hexapole and octopole superposition has been adopted to represent field inhomogeneities. A uniform charge density distribution has been assumed for characterizing space charge. Dipolar excitation has been represented as a forcing term weighted by dipole superposition, and damping is represented in terms of reduced collision frequency in the equation of ion motion. The perturbed secular frequency of the ion has been obtained by using a modified Lindstedt–Poincaré perturbation technique. The expression for perturbed frequency adequately reflects the reported experimental and simulation results. Perturbation is sign sensitive for octopole superposition and sign insensitive for hexapole superposition. Larger shifts occur with octopole aberrations. Perturbation of secular frequency based on the number of ions is mass dependent. Lower masses show larger negative frequency shifts with an increase in the number of ions within the trap. Dipolar excitation potential shifts the secular frequency in the positive direction and is larger for lower masses than for higher masses. Damping plays a minor role in shifting the secular frequencies. The shift increases as we increase the pressure of the bath gas. The shift in ion secular frequency with the axial distance from the center of the trap shows quadratic variation. (Int J Mass Spectrom 197 (2000) 263–278) © 2000 Elsevier Science B.V.

Keywords: Nonlinear traps; Perturbed secular frequency; Frequency shift; Space charge; Duffing equation

1. Introduction

The fundamental motional frequency of ions in the axial and radial directions in an ideal Paul trap, referred to as the ion secular frequency, ω_u, is computed from the equation

$$\omega_u = \beta_u \Omega / 2 \tag{1}$$

where Ω is the angular frequency of the rf drive potential applied to the central ring electrode and β_u is a parameter determined from the Mathieu parameters a_u and q_u where the subscript u refers to axial and radial directions. β_u is computed either from an implicit expression involving β_u, a_u, and q_u related by a continuous fraction relationship [1,2], or in

* Corresponding author. E-mail: agmenon@isu.iisc.ernet.in

PII S1387-3806(99)00265-1

pseudopotential well approximation when the value of q_u is less than 0.4, it can be computed from the adiabatic or Dehmelt approximation [3,4]

$$\omega_u = \left(a_u + \frac{q_u^2}{2} \right)^{1/2} \frac{\Omega}{2} \quad (2)$$

In ideal Paul traps, the field inside the trap varies linearly and the decoupled radial and axial equation of ion motion can be represented by the Mathieu equation [5,6]. In experimental traps, however, field distortions are caused by misalignment in the trap geometry and other factors, such as space charge and dipolar excitation, as in resonance ejection studies. Damping of ion motion due to the presence of buffer gas further complicates the equation of ion motion that now takes the form of a forced Duffing oscillator with damping. Some interesting consequences of having nonlinear terms in the equation of motion include perturbation of secular frequency from its ideal value [7,8], appearance of harmonics [9,10], coupling of secular frequency with the angular frequency of the rf drive [11], as well as coupling of radial and axial motion [12].

Perturbation of the secular frequency of ions in nonlinear Paul traps is a topic that has received considerable attention in literature, and will also be the focus of this article. Resonance ejection experiments [13] and broadband image current detection of ions [14] are examples of experiments in which the exact degree of frequency perturbation must be known for accurate mass assignment. The technique for generating tailored waveforms [15,16] for isolating targeted ions is another experiment where accurate frequency information is required for synthesizing a broadband excitation signal with a "notch" at the secular frequency of the targeted ions.

Several simulation studies are available in literature for characterizing the motion of ions in practical traps. Some of these include the integrated system for ion simulation (ISIS) program by Londry et al. [17], simulation program for quadrupole resonance (SPQR) by March et al. [18,19], and a multiparticle simulation program (ITSIM) for examining the effects of higher order fields, gas collisions, and ion–ion interactions in practical traps has been detailed by Bui and Cooks [20]. With the availability of clear experimental evidence of frequency perturbation in nonlinear Paul traps, we feel that it is now possible to correlate these observations into a single expression that relates the degree of frequency perturbation to experimental and practical constraints. Such an expression would help not only in developing an understanding of the interdependence of these effects but also, in a practical sense, offer a relationship that could be used to calibrate mass spectrometers. This article reports such an expression to understand the combined influence of geometric aberrations, space charge, dipolar excitation potential, and damping on the secular frequency of ions within a nonlinear Paul trap.

2. Method of analysis

To compute the perturbation in ion secular frequency caused by different experimental and practical constraints, we need to first develop an equation of motion that incorporates terms corresponding to geometric aberration, space charge, damping, and dipolar excitation. Such an equation will contain nonlinear terms arising due to field inhomogeneity, a damping term proportional to ion velocity, and a forcing term with an angular frequency corresponding to dipolar excitation. In nonlinear systems the natural frequency of the system will be different from the secular frequency of the ideal system (ω_0) by an amount that depends on the weights of the nonlinear superpositions [5]. In such systems it has been shown by Makarov [21] that the frequency at which energy is taken up by the oscillating ion is different from the ideal ion secular frequency and corresponds to the point on the frequency response curve at which the "jump" phenomenon occurs. In general, the shifted or perturbed frequency may be lower or higher than the ideal secular frequency depending on the specific inhomogeneities of the system and for resonance to occur in practical traps the frequency of dipolar excitation used in resonance ejection studies corresponds to this perturbed frequency. In what follows, we will present the expressions used in the present

study for characterizing geometric aberration, space charge, dipolar excitation, and damping that will be incorporated in the equation of ion motion within the trap.

2.1. Geometrical aberration

The potential distribution inside the trap due to rf potential can be represented by orthogonal Legendre polynomials with spherical and rotation symmetry in such a way that it satisfies the Laplace equation. In our computations, the weights of different multipoles are calculated using the data given by Beaty [22]. Wang et al. [23] and Brown and Gabrielse [24] have also followed a similar scheme to incorporate the multipole terms in the potential functions.

If P_n is the Legendre polynomial of order n, then the potential distribution inside the trap, $\phi(\rho, \theta, \varphi)$, in terms of spherical coordinates is given by

$$\phi(\rho, \theta, \varphi) = \phi_0 \sum_{n=0}^{\infty} A_n \frac{\rho^n}{r_0^n} P_n(\cos \theta) \tag{3}$$

where

$$\rho^2 = z^2 + r^2 \tag{4}$$

r and z are the radial and axial coordinates, respectively, and r_0 is the radius of the central ring electrode. A_n stands for the dimensionless weight factors for different terms. The various terms corresponding to $n = 0, 1, 2, 3 \ldots$ represent the multipole components of the potential. Although several higher order multipoles contribute to field inhomogeneity, from the point of simplicity of computations, in the present work, only two higher order multipoles viz. hexapole and octopole (corresponding to $n = 3$ and $n = 4$), are taken into account along with the quadrupole component for calculating the potential distribution inside the trap. ϕ_0 is the magnitude of the potential applied to the ring electrode. In our present computation we have assumed the operation of the trap along the $a_u = 0$ axis in the Mathieu stability plot, that is, when the dc potential is zero. Consequently,

$$\phi_0 = \mathrm{V}_0 \cos \Omega t \tag{5}$$

where V_0 is the 0-peak voltage of the rf potential. Upon expanding Eq. (3), we get the final expression for the potential distribution, $\phi_m(r, z, t)$, inside the trap due to hexapole and octopole superposition that is given by

$$\phi_m(r, z, t) = \frac{A_2}{r_0^2} \mathrm{V}_0 \cos \Omega t \left[z^2 - \frac{r^2}{2} + \frac{h}{r_0} \left(z^3 - \frac{3}{2} r^2 z \right) + \frac{f}{r_0^2} \left(z^4 - 3r^2 z^2 + \frac{3}{8} r^4 \right) \right] \tag{6}$$

where $h = A_3/A_2$ and $f = A_4/A_2$. Here A_2, A_3, and A_4 refer to the weight of the quadrupole, hexapole, and octopole superposition. The parameters f and h represent the strength of octopole and hexapole field superposition relative to the quadrupole contribution.

2.2. Space charge

The potential distribution due to the rf potential inside the trap gets distorted because of the defocusing caused by the coulombic repulsion effect between the ions when the ion density inside the trap is large. Different models have been used in literature for representing space charge density distribution. Li et al. [25], in their study of trapping force in Paul traps, have assumed a Boltzmann distribution for charge density. Vedel et al. [26], in their computational study, have adopted a Gaussian distribution model for calculating the spatial and energy probability densities of strongly confined ions in the presence of a light buffer gas. Meis et al. [27] and Parks and Szoke [28] have also used Gaussian distribution function for charge density while calculating the potential due to space charge. However, in resonance ejection studies [29], in collision activated dissociation studies [30], or in studies related to nondestructive measurement of ion secular frequencies [14] dipolar excitation applied across the endcap electrodes induces coherent motion [31] of the center of mass of the ion cloud leading to a more uniform charge distribution in the volume

traversed by the oscillating ions. Schuessler and Holder [32] have, for instance, suggested that at the time of detection, a charge distribution can be assumed uniform within the trapping volume. In the present work we have assumed a uniform charge distribution that produces a superimposed dc potential. The magnitude of the dc potential depends on the number of ions present in the trapping volume and for the axial direction it is given by [32,33]

$$U_{sc} = -\frac{z_0^2 N_{sc}}{4\varepsilon_0} \tag{7}$$

where

$N_{sc} = \text{eN}$

$e =$ charge of electron ($= 1.602 \times 10^{-19}$ C)

$N =$ number of ions per cm^3

$\varepsilon_0 =$ permittivity of free space

($= 8.854 \times 10^{-14}$ F/cm) (8)

2.3. Dipolar excitation

In resonance ejection experiments, the dipolar excitation potential applied to the endcap electrode distorts the electric field inside the trap. The pseudopotential well model [34] for three dimensional ion motion incorporates an excitation term in the ion motion equation for representing the excitation potential corresponding to the excitation potential $U_{\text{exc}}(r, z, t)$. This excitation term needs to be weighted by the dipolar superposition [23] and can be represented by

$$U_{\text{exc}}(r, z, t) = A_1 \text{V}_s \sin(\omega t)\left[\frac{z}{r_0}\right] \tag{9}$$

where A_1 is the weight of dipole superposition and can be calculated by the data given by Beaty [22] and ω is the angular frequency of the dipolar excitation potential that is applied to the endcap. It may be recalled that this angular frequency, ω, corresponds to the perturbed frequency of the ions within the non-ideal trap.

2.4. Damping

A buffer gas used for damping the ion motion inside the trap has been observed by Stafford et al. [35] to improve the resolution of the mass spectrum and the anharmonic motion of ions in Paul traps with light buffer gas has been studied by Sugiyama and Yoda [36]. Goeringer et al. [37] presented a method by which a damping term can be included in the equation of ion motion in terms of the reduced collision frequency. Makarov [21] has also used a similar expression to calculate the damping in terms of reduced collisional frequency, $c(du/dt)$, where c is given by

$$c = \frac{m_n}{m + m_n}\frac{p}{kT_b}\frac{e}{2\varepsilon_0}\sqrt{\alpha\frac{m + m_n}{mm_n}} \tag{10}$$

where m is the mass of analyte ion, m_n is the mass of neutral bath gas, α is the polarizability of the bath gas ($\alpha = 0.22 \times 10^{-40}$ Fm^2), ε_0 is the relative permitivity of the free space ($\varepsilon_0 = 8.854 \times 10^{-12}$ F/m), T_b is the temperature of the bath gas, and p is the pressure of the bath gas in Pascals. We have used this expression for computing the damping term.

3. Equation of ion motion

In classical mechanics, the three-dimensional motion of an ion within a pseudopotential well [34] with excitation potential applied to the endcap electrode is given by

$$m\frac{d^2\rho}{dt^2} + e\nabla U_{\text{eff}}(r, z) = -e\nabla U_{\text{exc}} \tag{11}$$

where ρ is the ion position vector and

$$U_{\text{eff}}(r, z) = \frac{1}{2}\frac{e}{m}\left\langle\left|\int_t \nabla\phi\, dt\right|^2\right\rangle \tag{12}$$

To evaluate U_{eff}, Eq. (6), is easily integrated under the assumption $\text{V}_0 \gg U_0$. When this assumption is made, U_{eff} takes the form

$$U_{\text{eff}}(r, z) = \frac{1}{8}\left(\frac{q_z^2\Omega^2}{8}\right) \times \left(\frac{m}{e}\right)\left(4z^2 + \frac{12h}{r_0}z^2 + \frac{16f}{r_0^2}z^4\right) \quad (13)$$

It may be seen that the first bracketed term in Eq. (13) corresponds to the square of the secular frequency of the ions (ω_0^2) in the absence of dc potential. However, since the dc bias produced by the space charge is equivalent to a dc potential applied across the endcap electrode [33] the secular frequency will now have to be computed from Eq. (2).

Substituting Eqs. (9) and (13) into Eq. (11) and including space charge and damping in the resulting equation, we get the following equation of ion motion in the axial direction

$$\frac{d^2z}{dt^2} + 2\mu\frac{dz}{dt} + \omega_0^2 z + \frac{9h}{2r_0}\omega_0^2 z^2 + \frac{8f}{r_0^2}\omega_0^2 z^3 = -F_s\cos(\omega t) \quad (14)$$

where

$$\omega_0^2 = \left(a_z + \frac{q_z^2}{2}\right)\frac{\Omega^2}{4} \quad (15)$$

$$a_z = \frac{8eU_{sc}}{mr_0^2\Omega^2}, \qquad q_z = \frac{4e\mathrm{V}_0}{mr_0^2\Omega^2} \quad (16)$$

$$F_s = \frac{eA_1\mathrm{V}_s}{mr_0} \quad (17)$$

$$\mu = \frac{c}{2} \quad (18)$$

One major approximation in the development of Eq. (14) is the omission of nonlinear coupling terms involving the radial coordinate. As has been pointed out in Sec. 1, practical traps have been known to produce coupling not only between rf drive frequency and secular motion but also coupling between radial and axial motion. The consequence of these couplings is the observation of sidebands on the rf drive frequency as well as harmonics [9,10] in secular motion and these observations in turn have been used to explain nonlinear resonances in practical traps. However, from the point of view of simplicity of analysis (coupled differential equations involving r^2z and z^2r terms, for instance, are not amenable to easy mathematical analysis) we have chosen to ignore terms involving radial coordinates.

It must also be emphasized here that Eq. (14) has been developed on the basic premise that the ions are oscillating in the trap within a pseudopotential well. Consequently, the results obtained in the present computations are valid for q_z values of up to 0.4.

4. Estimation of perturbed frequency, ω

For calculating the perturbed frequency ω from Eq. (14), we introduce a new dimensionless dependent variable x, with the substitution

$$z = xr_0 \quad (19)$$

Substituting (19) into Eq. (14) we get

$$\frac{d^2x}{dt^2} + 2\mu\frac{dx}{dt} + \omega_0^2 x + \alpha_2 x^2 + \alpha_3 x^3 = -k\cos(\omega t) \quad (20)$$

where

$$\alpha_2 = \frac{9h\omega_0^2}{2} \quad (21)$$

$$\alpha_3 = 8f\omega_0^2 \quad (22)$$

$$k = \frac{F_s}{r_0} \quad (23)$$

The final equation of motion of the ions in the axial direction has the form

$$\ddot{z} + \eta\dot{z} + F(z) = G(t) \quad (24)$$

where η is the damping constant, $F(z)$ is the restoring term, and $G(t)$ is the forcing term. In mathematical literature, equations of this form are known as forced Duffing equations with damping [38,39]. The solution to this type of Duffing equation without damping using a perturbation technique has been discussed for linear and cubic terms in the restoring term by Nayfeh

[40] and Frehlich and Novak [41] and for linear and quadratic terms by McLachlan [5]. Nayfeh and Mook [42] have dealt with the case of a system having quadratic nonlinearity along with the linear and cubic terms in the restoring terms, as occurs in betatron oscillations. In an earlier study [43] we had adopted the Lindstedt–Poincaré technique for the Duffings equation without damping. However, we found it difficult to extend this technique to obtain an expression for perturbed secular frequency in the present case for three reasons. First, using this method, we get an implicit expression involving perturbed frequency. Second, since a large number of effects are incorporated in the equation of ion motion, they all need to be ordered if their relative contributions are to be simultaneously perceived. And finally, because the Lindstedt–Poincaré technique used by us earlier demands that the perturbation parameter be small, we cannot a priori ascertain the strength of this parameter when all nonlinear effects are involved. In view of these observations, we chose a modified Lindstedt–Poincaré technique proposed by Cheung et al. [44] and an ordering scheme proposed by Nayfeh and Mook [42].

The basic assumption of the Lindstedt–Poincaré perturbation technique to the solution of the differential equation is to assume that the nonlinear terms in Eq. (20) change the secular frequency of the system from its ideal value of ω_0 to perturbed secular frequency ω. Before applying perturbation it is necessary to order the damping coefficient, the nonlinearity, and the external excitation in such a way that their effects appear simultaneously in the same perturbation scheme. Following Nayfeh and Mook [42], if we let $x = \epsilon u$ (where u is also a dimensionless displacement) it is necessary to order damping as $\epsilon^2 u$ and excitation as $\epsilon^3 k \cos(\omega t)$. This ordering scheme is valid for the primary resonance condition (that is, when $\omega \cong \omega_0$). With this ordering scheme the equation of ion motion becomes

$$\frac{d^2u}{dt^2} + 2\epsilon^2\mu \frac{du}{dt} + \omega_0^2 u + \epsilon\alpha_2 u^2 + \epsilon^2\alpha_3 u^3 = -\epsilon^2 k \cos(\omega t) \tag{25}$$

Here ϵ is a small dimensionless parameter. It is introduced into the above equation as a book-keeping device [45], and will be set to unity in the final solution.

The first step in the Lindstedt–Poincaré method is to introduce a dimensionless time τ into the Eq. (25) by means of the following transformation

$$\tau = \omega t, \tag{26}$$

which changes Eq. (25) into

$$\omega^2 \frac{d^2u}{d\tau^2} + 2\mu\omega\,\epsilon^2 \frac{du}{d\tau} + \omega_0^2 u + \epsilon\alpha_2 u^2 + \epsilon^2\alpha_3 u^3 = -\epsilon^2 k \cos\tau \tag{27}$$

In the normal Lindstedt–Poincaré perturbation procedure, ϵ is chosen as a perturbation parameter for solving Eq. (27) and the variables ω and u are expanded as an asymptotic series in terms of ϵ as

$$\omega = \sum_{n=0}^{\infty} \epsilon^n \omega_n \tag{28}$$

$$u = \sum_{n=0}^{\infty} \epsilon^n u_n \tag{29}$$

Because of the ordering scheme we followed, ω_1 becomes zero in the conventional Lindstedt–Poincaré method. Consequently, in the modified Lindstedt–Poincaré method a new scaled perturbation parameter γ in terms of ω_2 is introduced in accordance with [44] and is given by

$$\gamma^2 = \frac{\epsilon^2\omega_2}{\omega_0^4 + \epsilon^2\omega_2} \tag{30}$$

This requires the frequency ω to be expressed as the fourth power in the asymptotic series expansion involving the new perturbation parameter γ. The asymptotic series expansion for the variables ω and u in terms of the new perturbation parameter γ are given by [44]

$$\omega^4 = \frac{\omega_0^4}{1-\gamma^2}(1 + \delta_3\gamma^3 + \delta_4\gamma^4 + \ldots) \tag{31}$$

$$u = \sum_{n=0}^{\infty} u_n \gamma^n \tag{32}$$

Here δ_i's are the coefficients of the higher order perturbation parameter γ that must be determined for computing the perturbed frequency. However, because we have truncated the series up to and inclusive of γ^2 in our computation, we do not need to calculate δ_i's. With the introduction of the new perturbation parameter γ, the solution will be valid even if ϵ is very large, because $\gamma \rightarrow 1$ as $\epsilon \rightarrow \infty$.

In order to compute ω_2, Eqs. (31) and (32) are substituted into Eq. (27), and the coefficients of like powers of γ are equated. Thus we get a set of differential equations that can be successively solved for u_n and ω_2 by assuming a general solution [44] as

$$u_0 = A \cos \omega t + B \sin \omega t \tag{33}$$

where A and B are dimensionless arbitrary numbers. The value of ω_2 can now be derived as [46]

$$\omega_2 = \left\{ \frac{3}{2} \omega_0^2 \alpha_3 (A^2 + B^2) - \frac{10}{6} \alpha_2^2 (A^2 + B^2) \right\} + \frac{4\omega_0^3 \mu B}{A} + \frac{2\omega_0^2 k}{A} \tag{34}$$

where

$$A = \frac{z}{r_0} \tag{35}$$

$$B = \frac{-k + \sqrt{k^2 - 16\omega_0^2 \mu^2 A^2}}{4\omega_0 \mu} \tag{36}$$

In our calculation we have assumed the ion to be near the surface of the endcap electrode (i.e. $z = z_0$) where the nonlinearity will be maximum. There is one point to be noted in Eq. (36) in relation to our choice of the sign of the discriminant. We have used the positive sign for the discriminant for computing B because using the negative sign gave unobserved large frequency shifts.

Neglecting the powers of γ more than two in Eq. (31), we get the following as the final expression for the perturbed frequency ω:

$$\omega = \omega_0 \left[1 + \left(\frac{\omega_2}{4(\omega_0^4 + \omega_2)} \right) \right] \tag{37}$$

5. Contribution of trap nonideality to frequency perturbation

Before we go into the details of the influence of nonidealities of the practical trap on perturbing ion axial secular frequency we will digress in order to understand what Eq. (37) signifies in practical traps. This will also help us to test the conformity of our results to those available in mathematical literature.

It is well known in mechanical systems [5] as well as in nonlinear Paul traps [21] that nonidealities in the equation of ion motion distorts the normally symmetric amplitude frequency curve (referred to as the frequency response curve in literature). The magnitude of the response curve as well as its specific shape depends on the excitation force as well as the weights and the sign of nonlinear terms. These curves have been used to explain mass resolutions observed in forward and reverse scans in practical traps based on the "jump" phenomenon known to be exhibited by nonlinear systems [21].

In order to have physical insight as to what the perturbed frequency we developed means in the context of nonideal Paul traps we will rewrite Eq. (37) to take the form of a frequency response curve. This is done by first expressing Eq. (37) in terms of ω^2 as

$$\omega^2 = \omega_0^2 \left[1 + \left(\frac{\omega_2}{(\omega_0^4 + \omega_2)} \right) \right]^{1/2} \tag{38}$$

Next, we expand the square bracket as a power series up to the first term to get,

$$\omega^2 = \omega_0^2 \left[1 + \left(\frac{\omega_2}{2(\omega_0^4 + \omega_2)} \right) \right] \tag{39}$$

In order to compare our results with the well studied example we restrict our system to an example in mathematical literature [5] by setting damping, space charge, and hexapole term to zero (i.e. N, c, $\alpha_2 = 0$) and consider only the octopole superposition and dipolar excitation. Further, because ω_2 is very

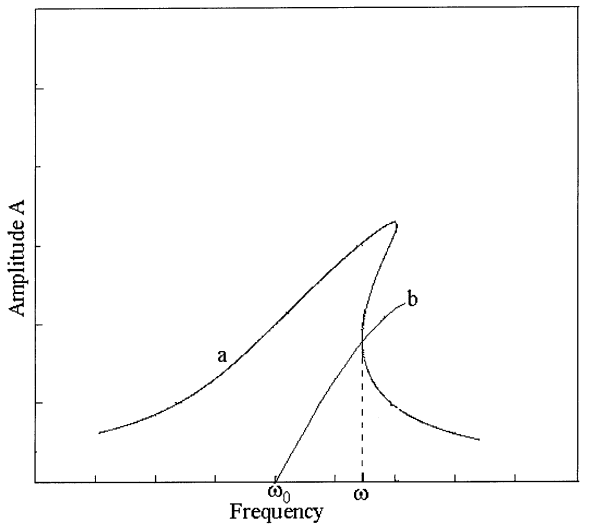

Fig. 1. Figure shows the frequency response and jump phenomenon of Eq. (40).

small compared to ω_0^4 in the denominator in Eq. (38), ω_2 is also ignored. With these substitutions Eq. (39) reduces to

$$\omega^2 = \omega_0^2\left[1 + \frac{3\alpha_3 A^2}{4\omega_0^2} + \frac{k}{\omega_0^2 A}\right] \tag{40}$$

This expression is identical to the expression developed by McLachlan [5] and corresponds to the frequency response curve for a forced Duffing equation with cubic nonlinearity. This equation is cubic in A and the real roots have the form shown in curve (a) of Fig. 1. A family of such curves are obtained for different values of dipolar excitation amplitude. All these curves show the humpback nature with the direction of the skew being determined by the sign of the octopole superposition.

To identify the stationary point where the tangent becomes parallel to the A axis corresponding to the jump phenomenon, following McLachlan [5], we differentiate Eq. (40) with respect to A (i.e. $d\omega/dA$) and equate the resulting expression to zero. By doing this we get

$$\frac{6\alpha_3 A^2}{4\omega_0^2} = \frac{k}{A} \tag{41}$$

Substituting Eq. (41) into Eq. (40) we obtain an expression for ω^2, which is given by

$$\omega^2 = \omega_0^2 + \frac{9\alpha_3 A^2}{4\omega_0^2} \tag{42}$$

Eq. (42) is again identical to the expression developed by McLachlan [5] and represents both the perturbed frequency as well as the loci of the stationary points at which the jump phenomenon takes place in non-linear Paul traps. This curve has been plotted as curve (b) in Fig. 1.

A second example of the conformity of Eq. (37) to results in mathematical results is to consider the case when damping, dipolar excitation, and space charge are set to zero. Eq. (37) now takes the form

$$\omega = \omega_0\left[1 + \frac{(9\omega_0^2\alpha_3 - 10\alpha_2^2)A^2}{24\omega_0^4}\right] \tag{43}$$

that is identical to the expression we derived in a previous work [43] and developed in Nayfeh [40] for a free Duffing oscillator with quadratic and cubic nonlinearity.

Eq. (37) is an expression of the contribution of geometric aberration, space charge, damping, and dipolar excitation to the overall frequency perturbation. Whereas Eq. (37) will be used in all computations below, in this section, in order to understand the effect of different parameters on perturbing the secular frequency, Eq. (34) will be adequate to study the details of each term of ω_2.

Different terms in Eq. (34) represent the shifts in the axial secular frequency caused by a combination of nonidealities. We will now examine the terms of Eq. (34) one by one in the following paragraphs.

The first term in Eq. (34) after the substitution of appropriate values for different variables is given by

$$12\omega_0^4 f\left[\frac{z^2}{r_0^2} + \left(\frac{-\dfrac{eA_1V_s}{mr_0^2} + \dfrac{1}{r_0}\sqrt{\dfrac{e^2A_1^2V_s^2}{m^2} - 4\omega_0^2c^2z^2}}{2\omega_0 c}\right)^2\right] \tag{44}$$

The above expression represents the effect of octopole superposition on secular frequency. It shows that the shift in secular frequency varies linearly with the strength f of octopole superposition. This term also indicates that the shift in secular frequency is dependent on the sign of octopole superposition. The shift will increase from its ideal value if the octopole superposition is positive and decrease from its ideal value if it is negative. The first term inside the square bracket (z^2/r_0^2) implies that the shift in secular frequency depends on the axial position of the ion and that it will be maximum when the ions are near the surface of the endcap electrodes (i.e. $z = z_0$). The second term inside the square bracket arises because of excitation and damping. This term is at its maximum value when the discriminant is zero and minimum when damping is zero. Because c is related to pressure through Eq. (10), an increase in the pressure of the damping gas increases the shift in secular frequency. In the absence of damping, the excitation potential will not have any effect on this term and the shift will be entirely due to the strength f of octopole superposition.

The second term in Eq. (34) when expanded takes the following form

$$-\frac{10}{6}\left(\frac{9h\omega_0^2}{2}\right)^2\left(\frac{z^2}{r_0^2}+\left(\frac{-\dfrac{eA_1V_s}{mr_0^2}+\dfrac{1}{r_0}\sqrt{\dfrac{e^2A_1^2V_s^2}{m^2}-4\omega_0^2c^2z^2}}{2\omega_0 c}\right)^2\right) \quad (45)$$

The above expression indicates that secular frequency varies quadratically with the hexapole weight factor h and consequently is insensitive to the sign of the superposition. Because Eq. (45) has a negative sign, the shift will increase in the negative direction with an increase in the hexapole superposition. The above expression also shows that under a fixed set of experimental conditions, the shift in secular frequency will be governed by the axial position of the ions, the amplitude of the excitation potential, and the pressure of the neutral bath gas.

When the third term in Eq. (34) is expanded we get

$$\left(\frac{\omega_0^2 r_0}{z}\right)\left[-\frac{eA_1V_s}{mr_0^2}+\frac{1}{r_0}\sqrt{\frac{e^2A_1^2V_s^2}{m^2}-4\omega_0^2c^2z^2}\right] \quad (46)$$

This term makes a contribution to the frequency perturbation through the magnitude of dipolar excitation, position, ion mass, and damping. In the absence of damping this term does not contribute to frequency perturbation. It may be noted that the first part of Eq. (46) is identical to (with a negative sign and half its magnitude) the fourth term of Eq. (34), which is expanded below:

$$\frac{2\omega_0^2 eA_1V_s}{mr_0 z} \quad (47)$$

Eq. (46) will have a maximum value when the discriminant of B is zero, that is, when $eA_1V_s/m = 2\omega_0 cz$. Under this condition the net contribution of Eqs. (46) and (47) will be half the magnitude of Eq. (47) and the frequency perturbation will vary linearly with dipolar excitation.

6. Results and discussion

It is evident from Eq. (37) that in practical traps the perturbation in secular frequency arises out of a complex interplay of different experimental parameters. Four of these parameters are incorporated in the equation of motion in the present article. In order to test the conformity of the expression we derived to the reported experimental and simulation observations, we plotted curves representing the variations in frequency with the different experimental parameters. Most of the figures represent perturbed frequency as a ratio, ω/ω_0, whereas Figs. 5 and 9 represent the perturbed frequency as $(\omega - \omega_0)$ for the purpose of clarity. Figs. 2–4 brings out the frequency perturbation due to geometric aberration. Fig. 5 indicates the effect of charge density within the trap whereas Figs. 6 and 7 indicate frequency perturbation due to dipolar excitation potential. Figs. 8 and 9 show the variation of frequency perturbation due to damping and axial position of the ions, respectively. In all the figures, unless specified otherwise, the variables have the following values: $f = h = 0.01$, $V_s = 300\ mV_{0-p}$,

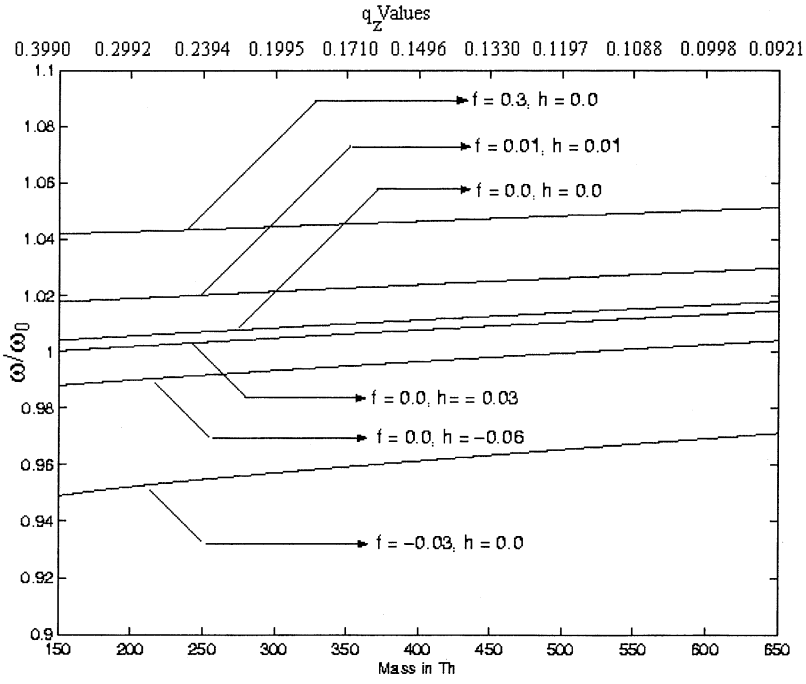

Fig. 2. Shift of secular frequency for different values of multipole superposition when $V_{rf} = 300\ V_{0-p}$.

$p = 3 \times 10^{-6}$ Pascal, $\Omega = 1.0$ MHz, and $V_{rf} = 300\ V_{0-p}$.

Fig. 2 shows the shift in secular frequency (ω/ω_0) versus mass for different values of multipole superposition. In these curves V_{rf} has been fixed at 300 V_{0-p} and each mass is oscillating at its own secular frequency corresponding to this potential (for instance secular frequency ω_0 for 300 Th corresponding to a drive potential of 300 V_{0-p} is 71.1 kHz with $q_z = 0.1995$, whereas ω_0 for 600 Th is 35.3 kHz with $q_z = 0.0998$). From Fig. 2 it can be seen that positive octopole superposition shifts the secular frequency in the positive direction whereas the hexapole superposition shifts the secular frequency in the negative direction. Similar behavior was also reported by Franzen [47,48] and Franzen et al. [11] in their simulation studies. It can also be observed that for a given weight of hexapole and octopole superposition, octopole superposition plays a dominant role in shifting the secular frequency. This plot also shows the dependence of secular frequency shift on the sign of the octopole superposition (curves corresponding to $f = +0.03$ and $f = -0.03$). The effect of hexapole superposition on shifting the secular frequency is weaker than the effect produced by negative octopole superposition (curves corresponding to $f = -0.03$, $h = 0$, and $f = 0.0$, $h = 0.3$). These observations match the results obtained by Franzen [48] in his studies of mass selective instability scan with multipole superposition. Cox et al. [49] have also found mass-dependent mass shifts in their study of characteristics of quadrupole ion traps at high resolution. The small shift observed in the curve even when there is no field aberration, i.e. when $f = h = 0$, is caused by excitation potential and damping.

Fig. 3 is a plot of the shift in secular frequency (ω/ω_0) versus mass at different multipole superpositions when ω_0 is fixed at 100 kHz for all masses. In these computations, V_{rf} is varied in the computations in order to bring the secular frequency of each mass to resonate with the dipolar excitation. This is a situation encountered in resonance ejection experiments. This plot is intended to show that for a given mass, the frequency shift will be different at different q_z values

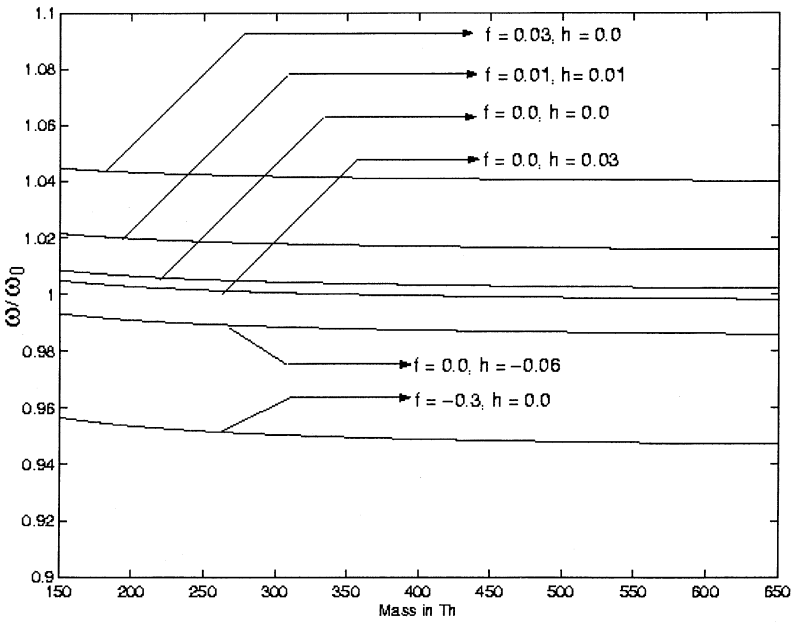

Fig. 3. Shift of secular frequency for different values of multipole superposition when $\omega_0 = 100$ kHz for all masses.

on the Mathieu stability plot. This may be seen by contrasting Fig. 3 with Fig. 2. The value of ω/ω_0 at mass 300 Th in Fig. 3 (plotted for $q_z = 0.2784$) is 1.018 for the curve corresponding to $f = h = 0.01$, whereas its ω/ω_0 value is 1.021 when $q_z = 0.1995$ (in Fig. 2) for the same field aberration. The effect of frequency shifts at different secular frequencies of 50 kHz ($q_z = 0.1408$), 100 kHz ($q_z = 0.2784$), and 150 kHz ($q_z = 0.4094$) for different masses may be seen in Fig. 4. Here the field aberration has been kept at $f = h = 0.01$ and the excitation potential is fixed at 0.5 V_{0-p}. In this plot it can be seen that at a particular operating point, the shift in secular frequency is higher at lower masses than at higher masses. These observations are of relevance when choosing dipolar excitation frequencies in resonance ejection experiments.

We next turn our attention to the effect of charge density on frequency perturbation. Dawson [4] has investigated the space charge limit within the Paul trap using the Dehmelt model that invokes the Poisson relation and has estimated that the maximum ion density within the trap is of the order of 10^7 ions/cm^3. In view of this we have plotted in Fig. 5 ($\omega - \omega_0$) values for a situation when the number of ions within the trap varies from 10^6 to 10^7.

Here too the computations have been done keeping the resonance ejection experiments in mind, and the unperturbed secular frequency of the ions has been fixed at 100 kHz. Nappi et al. [14], reporting on their image detection studies of frequency shift due to space charge, observed that there will be a decrease in frequency in ion oscillations when the number of ions inside the trap increases (see Fig. 5 for masses 100, 300, 500, 750, and 1000 Th). It can be seen that the perturbation in the secular frequency is higher for lower masses than for higher masses. Further, the perturbation increases linearly with an increase in the number of ions. The effect of space charge in shifting ion secular frequency has been shown to be mass dependent by Todd et al. [50] in their experimental studies. A similar observation has also been made by Fulford et al. [51] while studying the resonance ejection of ions in a 3-D quadrupole ion trap.

Fig. 6 represents the effect of the magnitude of dipolar excitation potential on the ion secular fre-

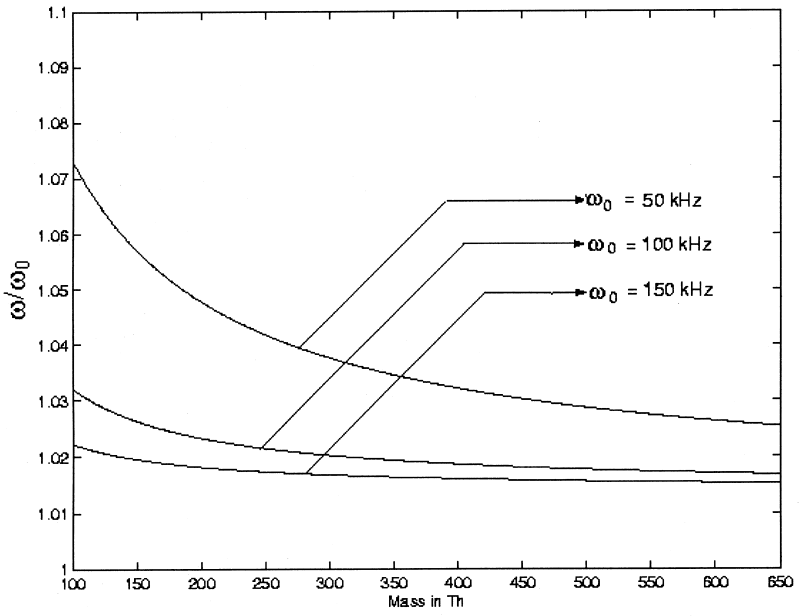

Fig. 4. Shift of secular frequency at different operating points in the Mathieu stability plot.

quency. It may be recalled that this potential has the effect of distorting the electric field inside the trap leading to perturbation in secular frequency. Curves have been plotted for a variation of V_s from 0.3 to 1 V_{0-p} and for masses corresponding to 300, 500, 750, and 1000 Th. It may be seen that higher excitation

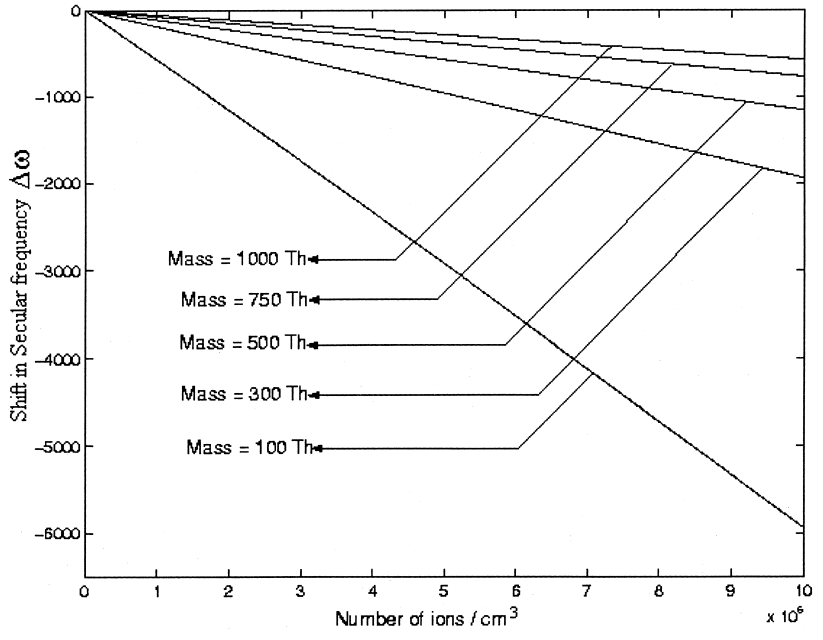

Fig. 5. Shift of secular frequency vs. the number of ions in the trap.

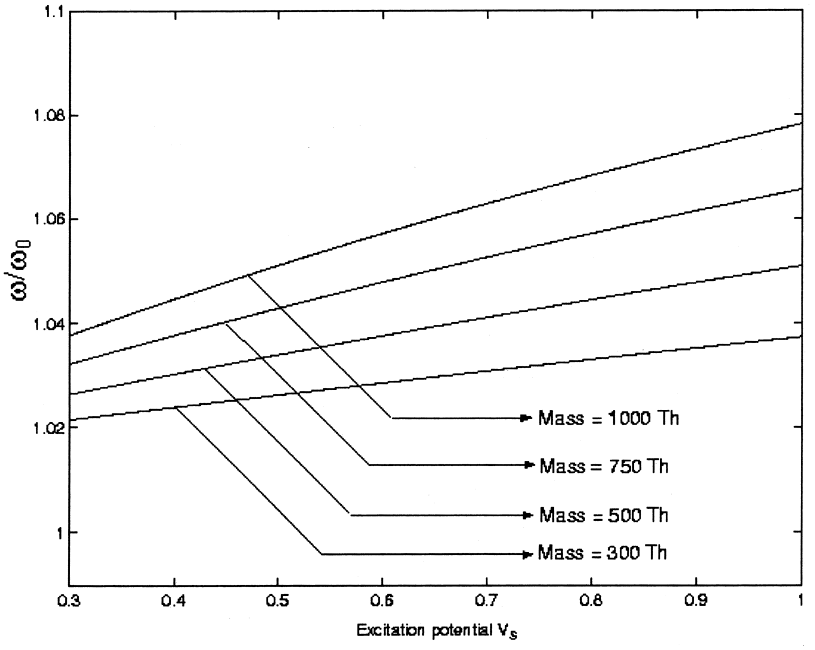

Fig. 6. Shift of secular frequency for different values of dipolar excitation when $V_{rf} = 300\ V_{0-p}$.

voltages increase the shift in ion secular frequencies irrespective of ion mass. For a given value of the dipolar excitation potential and other nonlinear parameters, at a given operating point in the Mathieu stability plot, the shift in the secular frequency should be larger for lower masses than for higher masses (as seen in Fig. 4). Kaiser et al. [52] and Cox et al. [49] have reported mass shift caused by dipolar excitation in resonance ejection studies in nonlinear Paul traps where ion energetics have been used to account for the larger delay in ejection of higher masses in contrast to lower masses at a fixed operating condition. In a specific experiment, Kaiser et al. [52] have pointed out that lower masses experience larger absolute mass shifts in contrast to higher masses where the apparent mass shift is lower. Fig. 7 provides more detailed insight as to the perturbation of ion secular frequency when a particular mass is oscillating at a different q_z value on the Mathieu stability plot. The different plots in this figure show frequency shifts for mass 300 Th when ω_0 is 50 kHz ($q_z = 0.1408$), 100 kHz ($q_z = 0.2784$), and 150 kHz ($q_z = 0.4094$). This plot also shows that as q_z increases the dependence of frequency shift on excitation potential becomes less pronounced.

Fig. 8 shows the variation of ω/ω_0 for different masses under different values of the bath gas pressure when ω_0 is fixed at 100 kHz ($q_z = 0.2784$) and $V_s = 300\ mV_{0-p}$. As the pressure increases for a given dipolar excitation potential, the shift in secular frequency also increases for all masses. Although there is a perceptible difference at higher masses, the difference is negligible at lower masses. Guan and Marshall [25] have also discussed the effect of bath gas pressure shifting the ion secular frequency. In their study too, it has been seen that an increase in pressure results in larger frequency shifts although the shift is in the negative direction. This negative shift may also be anticipated in our computation from a study of Eq. (36). However, because dipolar excitation potential also plays a part in perturbing the secular frequency (Figs. 6 and 7) the overall shift due to increase in pressure at a fixed dipolar excitation potential results in a shift in the positive direction.

Finally, Fig. 9 shows the absolute shift in secular frequency ($\omega - \omega_0$) with respect to the axial position

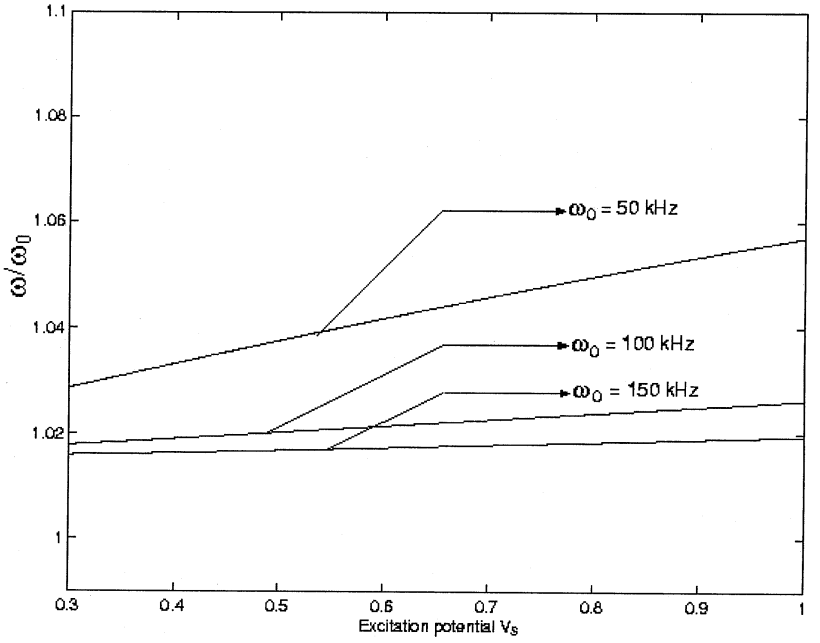

Fig. 7. Shift of secular frequency for $m = 300$ Th at different operating points in the Mathieu stability plot.

for ions of different mass when ω_0 is fixed at 100 kHz ($q_z = 0.2784$). The y axis shows an absolute value of shift in secular frequency (in Hz) because the difference could not easily be seen in a ω/ω_0 plot. For generating these curves, we have assumed that there is no excitation or damping. The shift, which is zero at

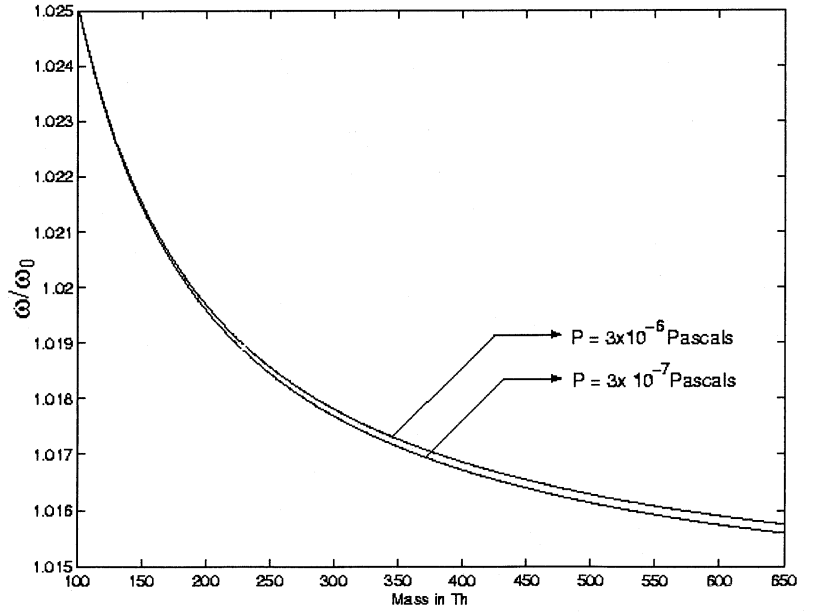

Fig. 8. Shift of secular frequency for different pressures of damping bath gas.

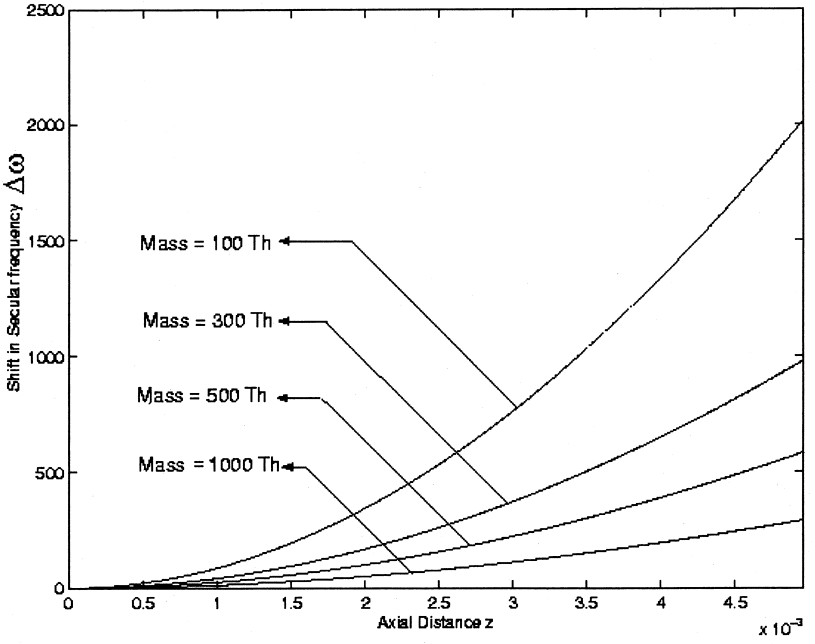

Fig. 9. Shift of secular frequency for different masses at different axial positions.

the center of the trap (i.e. the field is purely quadrupolar), increases as the axial distance increases. This was pointed out by Franzen [47] in his simulation studies of an ion cage with superimposed multipole fields. A similar result was obtained by Splendore et al. [53] in their simulation study of ion kinetic energies during resonance excitation experiments. Fig. 9 also shows that the shift in secular frequency increases with an increase in the axial distance–more in the case of lower masses than with higher masses.

Acknowledgements

We gratefully acknowledge the help received from Professor Mythily Ramaswamy, the TIFR-IISc Joint Mathematics Programme for discussions on the perturbation technique, and from Professor Thomas Chacko of our Institute for copyediting the manuscript. The manuscript has also benefitted from the suggestions offered by Dr. N. Chandrasekhar and Umakanth Rapol, Department of Physics. We would also like to thank three anonymous reviewers for their pertinent criticisms. Specifically, the discussion on the jump phenomenon and the uniform space charge distribution model was prompted by queries raised by them in our original manuscript.

References

[1] R.E. March, R.J. Hughes, Quadrupole Storage Mass Spectrometry, Wiley, New York, 1989.
[2] R.E. March, Int. J. Mass Spectrom. Ion Processes 118/119 (1992) 72.
[3] R.F. Wuerker, H. Shelton, R.V. Langmuir, J. Appl. Phys. 30 (1959) 342.
[4] P.H. Dawson, Quadrupole Mass Spectrometry and Its Application, Elsevier, Amsterdam, 1976.
[5] N.W. McLachlan, Ordinary Non-linear Differential Equations in Engineering and Physical Sciences, Oxford University Press, UK, 1958.
[6] M. Abromowitz, I.A. Stegun, Handbook of Mathematical Functions, Dover, New York, 1970.
[7] J. Yoda, K. Sugiyama, Japan J. Appl. Phys. 31 (1992) 3744–3749.
[8] X. Luo, X. Zhu, K. Gao, J. Li, M. Yan, L. Shi, J. Xu, Appl. Phys. B 62 (1996) 421.
[9] R. Alheit, S. Kleineidam, F. Vedel, M. Vedel, G. Werth, Int. J. Mass Spectrom. Ion Processes 154 (1996) 155.

[10] X.Z. Chu, M. Holzki, R. Alheit, G. Werth, Int. J. Mass Spectrom. Ion. Processes 173 (1998) 107.
[11] J. Franzen, R.H. Gabling, M. Schubert, Y. Wang, in R.E. March, J.F.J. Todd (Eds.), Practical Aspects of Ion Trap Mass Spectrometry, CRC, New York, 1995, Chap. 3, p. 49.
[12] M. Vedel, J. Rocher, M. Knoop, F. Vedel, Appl. Phys. B 66 (1998) 191.
[13] J.D. Williams, K.A. Cox, R.G. Cooks, S.A. McLuckey, K.J. Hart, D.E. Goeringer, Anal. Chem. 66 (1994) 725.
[14] M. Nappi, V. Frankevich, M. Soni, R.G. Cooks, Int. J. Mass Spectrom. Ion Processes 177 (1998) 91.
[15] S. Guan, A.G. Marshall, Anal. Chem. 65 (1993) 1288.
[16] R.K. Julian, R.G. Cooks, Anal. Chem. 65 (1993) 1827.
[17] F.A. Londry, R.L. Alfred, R.E. March, J. Am. Soc. Mass. Spectrom 4 (1993) 687.
[18] R.E. March, A.W. McMahon, F.A. Londry, R.L. Alfred, J.F.J. Todd, F. Vedel, Int. J. Mass Spectrom. Ion Processes 95 (1989) 119.
[19] R.E. March, A.W. McMahon, E.T. Allinson, F.A. Londry, R.L. Alfred, J.F.J. Todd, F. Vedel, Int. J. Mass Spectrom. Ion Processes 99 (1990) 109.
[20] H.A. Bui, R.G. Cooks, J. Mass Spectrom. 33 (1998) 297.
[21] A.A. Makarov, Anal Chem. 68 (1996) 4257.
[22] E.C. Beaty, Phys. Rev. A 33 (1986) 3645.
[23] Y. Wang, J. Franzen, K.P. Wanczek, Int. J. Mass Spectrom. Ion Processes 124 (1993) 125.
[24] L.S. Brown, G. Gabrielse, Rev. Mod. Phys. 58 (1986) 233.
[25] G-Z. Li, S. Gaun, A.G. Marshall, J. Am. Soc. Mass Spectrom. 9 (1998) 473.
[26] F. Vedel, J. Andre, M. Vedel, G. Brincourt, Phys. Rev. A 27 (1983) 2321.
[27] C. Meis, M. Desaintfuscien, M. Jardino, Appl. Phys. B 45 (1988) 59.
[28] J.H. Parks, A. Szoke, J. Chem. Phys. 103 (1995) 1422.
[29] R.L. Alfred, F.A. Londry, R.E. March, Int. J. Mass Spectrom. Ion Processes 125 (1993) 171.
[30] J.N. Louris, R.G. Cooks, J.E.P. Syka, P.E. Kelley, G.C. Stafford Jr., J.F.J. Todd, Anal. Chem. 59 (1987) 1667.
[31] D.E. Goeringer, R.I. Crutcher, S.A. McLuckey, Anal. Chem. 67 (1995) 4164.
[32] H.A. Schuessler, C.H. Holder Jr., J. Appl. Phys. 50 (1979) 5110.
[33] E. Fischer, Z. Phys. 156 (1959) 1.
[34] L.D. Landau, E.M. Lifshitz, Mechanics, Third Edition, Pergamon, UK, 1976.
[35] G.C. Stafford Jr., P.E. Kelley, J.E.P. Syka, W.E. Reynolds, J.F.J. Todd, Int. J. Mass Spectrom. Ion Processes 60 (1984) 85.
[36] K. Sugiyama, J. Yoda, Appl. Phys. B 51 (1990) 146.
[37] D.E. Goeringer, W.B. Whitten, J.M. Ramsey, S.A. McLuckey, G.L. Glish, Anal. Chem. 64 (1992) 1434.
[38] A.H. Nayfeh, Perturbation Methods, Wiley, New York, 1973.
[39] K.O. Friedrichs, J.J. Stoker, Q. Appl. Math. 1 (1943) 97.
[40] A.H. Nayfeh, Problems in Perturbation, Wiley, New York, 1985.
[41] R.G. Frehlich, S. Novak, Int. J. Non-linear Mech. 20 (1985) 123.
[42] A.H. Nayfeh, D.T. Mook, Nonlinear Oscillations, Wiley, New York, 1979.
[43] S. Sevugarajan, A.G. Menon, Int. J. Mass Spectrom. 189 (1999) 53.
[44] Y.K. Cheung, S.H. Chen, S.L. Lau, Int. J. Non-linear Mech. 26 (1991) 367.
[45] A.H. Nayfeh, J. Sound Vib. 92 (1984) 363.
[46] S. Sevugarajan, Frequency Perturbation in Non-linear Paul Traps, unpublished M.Sc. (Engg) Thesis, Department of Instrumentation, Indian Institute of Science, Bangalore 560012, India (1999).
[47] J. Franzen, Int. J. Mass Spectrom. Ion Processes 106 (1991) 63.
[48] J. Franzen, Int. J. Mass Spectrom. Ion Processes 125 (1993) 165.
[49] K.A. Cox, C.D. Cleven, R.G. Cooks, Int. J. Mass Spectrom. Ion Processes 144 (1995) 47.
[50] J.F.J. Todd, R.M. Waldren, R.E. Mather, Int. J. Mass Spectrom. Ion Phys. 34 (1980) 325.
[51] J.E. Fulford, D.-N. Hoa, R.J. Hughes, R.E. March, R.F. Bonner, G.J. Wong, J. Vac. Sci. Technol. 17 (1980) 829.
[52] R.E. Kaiser Jr., R.G. Cooks, G.C. Stafford Jr., E.P. Syka, P.H. Hemberger, Int. J. Mass Spectrom. Ion Processes 106 (1991) 79.
[53] M. Splendore, F.A. Londry, R.E. March, R.J.S. Morrison, P. Perrier, J. Andre, Int. J. Mass Spectrom. Ion Processes 156 (1996) 11.